Chapter 04

Isolation of Asiatic acid and development of its EGFR targeted albumin nanoparticles, and their cytotoxicity and pharmacokinetics evaluation for lung cancer therapy

4 Chapter 04: Isolation of Asiatic acid and rational development of its EGFR targeted albumin nanoparticles, and their cytotoxicity and pharmacokinetics evaluation for lung cancer therapy

4.1 Objective

The objective of this study was to isolate Asiatic acid and to prepare Asiatic acid (ASA) loaded albumin nanoparticles (ALB-NPs) conjugated with cetuximab antibody for targeting EGFR receptors and to characterize the prepared nanoformulations on the basis of their physicochemical properties such as shape, particle size, zeta-potential, surface morphology and surface chemistry. Moreover, developed ALB-NPs were evaluated for *in vitro* cytotoxicity against A549 cells, and a safety assessment was carried out on HEK-293 cells; *in vivo* pharmacokinetics and histopathology studies were also performed.

4.2 Plan of study

1. Isolation and purification of Asiatic acid.

2. Preparation and characterization of ASA-loaded albumin nanoparticles (ASA-ALB-NPs) using emulsification -solvent evaporation method.

3. Preparation of CTX conjugated EGFR targeted CTX-ASA-ALB-NPs using acid-amine coupling reaction.

4. Physicochemical and *in vitro* evaluation of EGFR-targeted CTX-ASA-ALB-NPs and ASA-ALB-NPs. The following studies were performed.

- ✓ Particle size, polydispersity index, and zeta potential.
- ✓ Electron microscopy studies (TEM) & AFM study.
- ✓ Crystallographic studies by XRD.
- ✓ Surface chemistry by XPS.
- ✓ Determination of entrapment efficiency.

- ✓ *In vitro* drug release studies.
- ✓ *In vitro* cellular uptake study on A549 cells.
- ✓ *In vitro* cytotoxicity on A549 and HEK-293 cells.

6. *In vivo* evaluation of EGFR-targeted ALB-NPs.

- ✓ Pharmacokinetic studies in Wistar rats.
- ✓ Histopathology studies in Wistar rats.

4.3 Chemicals and reagents

N-(3-Dimethylaminopropyl)-N′-ethylcarbodiimide hydrochloride (EDC hydrochloride), N-hydroxysuccinimide (NHS), Vitamin E polyethylene glycol succinate (Vitamin E-TPGS), coumarin 6 (C6), Pur-A-Lyzer™ midi dialysis kit (capacity 50-800 µL, MWCO 1 kDa), and Bovine Serum Albumin (ALB) were purchased from Sigma Aldrich Chemicals Private Limited, Bengaluru, India. Merck Specialities Ltd. in Mumbai, India, provided Cetuximab, which is also known as Erbitux R. The national repository division of the National Centre for Cell Science (NCCS) in Pune, India, provided the A549 and HEK-293 cell lines. Dead cell apoptosis kits with Annexin V for flow cytometry, Dulbecco's modified Eagles medium (DMEM), Fetal bovine serum (FBS), 3-(4,5-dimethyl thiazolyl-2-yl)-2,5-diphenyltetrazolium bromide (MTT), and trypsin-EDTA were purchased from Thermo Fisher Scientific, Mumbai, India.

Tarsons Products Limited, Kolkata, India, supplied the 96-well culture plates and culture flasks with different capacities. High-performance liquid chromatography (HPLC)-grade acetonitrile and methanol were sourced from Merck, Darmstadt, Germany. Deionized water was prepared using a Milli-Q purification system from Millipore, Molsheim, France. Reagents, chemicals, and other consumables used anywhere else in conducting experiments were of molecular biology or analytical grade.

4.4 Methods

4.4.1 Extraction and isolation of Asiatic acid (ASA)

ASA was isolated from Shorea robusta resin through a previously documented procedure, incorporating slight adjustments (92). A 500 g quantity of dried powdered resin underwent a defatting process with petroleum ether over a 24-hour period. The resulting defatted residue was then extracted sequentially with ethyl acetate and methanol (3×5 L) at room temperature for 48 hours each time. The methanolic extract was subsequently dried under vacuum at 40 ºC - 45 ºC and separated into n-butanol and water fractions. The n-butanol portion, upon vacuum drying, yielded 165 g of material, which was further processed to isolate metabolites.

The crude residue from the n-butanol extract was subjected to column chromatography using silica gel (60-120 mesh). Elution was performed using chloroform, followed by different $CHCl_3$-MeOH mixtures (98:2, 95:5, 90:10, and 80:20). A total of 80 fractions (250 mL each) were collected, and fractions displaying similar spots on thin layer chromatography were combined. Fractions eluted with $CHCl_3$-MeOH (95:5) were pooled and subjected to re-chromatography over silica gel to obtain a colorless solid (0.042 %). The compound underwent further purification through re-crystallization using methanol.

After obtaining the crystalline product, the compound underwent characterization through analytical methods, such as high-resolution mass spectrometry (ESI-HRMS). The spectral findings were validated by comparing them with information documented in existing literature.

4.4.2 Molecular docking investigations

Molecular docking was conducted to explore the interaction between asiatic acid (the ligand) and proteins ALB (PDBID: 4JK4), bovine beta-lactoglobulin (PDBID: 3NPO), and bovine lactoferrin (PDBID: 1BLF). Auto Dock Vina (181) was employed for this purpose. The preparation of proteins and ligands utilized ADT tools with default settings. Initially, ligands were subjected to energy minimization using Chem 3D tools. Water molecules were removed,

AD4-type atoms were assigned, and polar hydrogen atoms were added. Interactions in 2D and 3D were generated using Biovia Discovery Studio 2021.

4.4.3 Preparation of TPGS- SA

The synthesis of the TPGS and SA (succinic anhydride) conjugate involved a reaction between TPGS (0.79 g, 1 mmol) and succinic anhydride (0.10 g, 2 mmol), conducted in the presence of a catalytic quantity of DMAP (1 mmol). This reaction occurred in dry DCM under inert conditions and was stirred for 24 hours at 100 ºC. Once the reaction was complete, the resulting mixture was allowed to cool to room temperature and subsequently precipitated using cold diethyl ether at -5 ºC. The resulting precipitate was then dissolved in DCM, and any undesired impurities were removed through repeated filtration. The resulting white TPGS-SA precipitate was subjected to vacuum drying and stored at -20 ºC for future use (148).

4.4.4 Characterization of TPGS-SA

The synthesized TPGS-SA was confirmed by analytical techniques such as Mass spectrometry. For Mass spectra, TPGS and TPGS-SA were dissolved in methanol and recorded by SCIEX X500r Q-TOF, a high-resolution mass spectrometry equipment. The acquisition of mass spectra was carried out in a range of mass-to-charge ratio (m/z) from 100 to 1800 Da. The obtained spectral data were authenticated by comparing with the previously reported literature.

4.4.5 Preparation and optimization of ASA-loaded ALB-NPs

The method employed to develop ASA-ALB-NPs involved using the emulsion-solvent evaporation technique (149). The procedure started with gathering all necessary ingredients listed in Table 9. ASA was dissolved in a 1 mL mixture of ethanol and chloroform (1:4) to create a 3 mg/mL ASA solution. Simultaneously, 30 mg of ALB was dissolved in distilled water, serving as the carrier for ASA delivery. TPGS (20 mg) or a combination of TPGS (10 mg) and TPGS-SA (10 mg) was added to the ALB solution under constant stirring (500 rpm, REMI magnetic stirrer). The ASA solution was then slowly introduced into the mixture and

stirred at 500 rpm for 15 minutes. The resulting solution underwent ultrasonication using a probe sonicator for 5 minutes. Finally, the chloroform and ethanol solvent mixture was removed from the synthesized albumin nanoparticles containing ASA (ASA-ALB-NPs) using a rotary evaporator.

The developed formulation underwent filtration using a 0.22 μm membrane syringe filter to achieve consistent particle size. Additionally, non-targeted albumin nanoparticles (ALB-NPs) were created by incorporating C6 instead of ASA through the identical method mentioned earlier, intended for cellular uptake studies. To eliminate larger particles from the NPs formulations, a 0.22 μm syringe filter was employed for filtration, followed by centrifugation at 8000 rpm for 15 minutes.

4.4.6 CTX conjugation to ASA-ALB-NPs

To prepare targeted CTX-ASA-ALB-NPs, a solution containing TPGS-SA incorporated NPs was stirred, and EDC and NHS were added in a molar ratio of 5:1. This mixture was then stirred for 45 minutes. Following that, Cetuximab (2.5 mg) was introduced into the reaction mixture and agitated for 30 minutes.

The unreacted reagents were eliminated from the NPs suspension through dialysis against an ASA-saturated solution for further analysis of cellular uptake. For this purpose, targeted CTX-ALB-NPs were loaded with C6 instead of ASA, following the same procedure. Lastly, the purification process was carried out via centrifugation at 8000 rpm for 15 minutes, followed by filtration through a 0.22 μm membrane.

Table 9 Preparation of non-targeted ALB-NPs and CTX-conjugated ALB-NPs formulations.

Batches	ALB (mg)	TPGS (mg)	TPGS-SA (mg)	ASA (mg)	CTX (mg)	C6 (mg)
ASA-ALB-NPs	30	20	-	3	-	-
CTX-ASA-ALB-NPs	30	10	10	3	2.5	-
C6-ASA-NPs	30	20	-	-	-	0.3
CTX-C6-ASA-NPs	30	10	10	-	2.5	0.3

ASA-ALB-NPs: Asiatic acid-loaded ALB-NPs
CTX-ASA-ALB-NPs: Asiatic acid loaded CTX conjugated ALB-NPs
C6-ALB-NPs: Coumarin-6 loaded ALB-NPs
CTX-C6-ALB-NPs: Coumarin-6 loaded CTX conjugated ALB-NPs

4.5 Characterization of the physicochemical properties of ALB-NPs.

4.5.1 Assessment of the charge, particle size, and polydispersity index of ALB-NPs.

The dynamic light scattering technique, employing the Zeta sizer (Nano ZS 90, Malvern Instruments, UK) at room temperature, was utilized to measure the zeta potential, hydrodynamic particle size, and polydispersity index (PDI) of ALB-NPs. Prior to conducting the measurements, the ALB-NPs were adequately diluted in ultrapure (Milli-Q) water (150).

4.5.2 Fourier Transform Infrared (FTIR) spectroscopy analysis

The analysis of chemical functionality and potential interactions among ASA, ALB, and TPGS was carried out using the FTIR Spectrometer (Nicolet™ iS™ 5 spectrometer, Thermo Fisher Scientific Instruments LLC, USA). Pure ASA, excipients, and the prepared NPs were separately mixed with potassium bromide of IR grade to create pellets (182). A hydraulic press (HP-15-TM) was employed to produce thin, transparent pellets with a force of 15.0 tons. Spectra were recorded by scanning each pellet individually over the infrared range from 4000 to 500 cm^{-1}.

4.5.3 X-ray diffraction (XRD) analysis

XRD analyses were conducted to explore the crystallinity of drugs, excipients, and the formulated ALB-NPs. Additionally, this study aimed to assess the integrity of the individual components within the sample. The Bench Top X-Ray Diffraction system (Rigaku, Japan) was utilized to generate diffractograms for ASA, ALB, ASA-ALB-NPs, and CTX-ASA-ALB-NPs. The diffractograms were obtained through X-ray scanning of samples over an angle range from $2\theta = 10^{o}$ to $2\theta = 100^{o}$, employing Cu source Kα ($\lambda = 1.54$ Å) as the radiation source. The scanning was performed at a rate of 10^{o}/ min, and a tube voltage of 40 kilovolts was applied (152).

4.5.4 Morphological analysis of ALB-NPs

4.5.4.1 Transmission electron microscopy (TEM) analysis

TEM studies were performed to observe the size, shape, and internal composition of ASA-ALB-NPs and CTX-ASA-ALB-NPs. This was done by diluting the particles with deionized water and placing a drop on a copper grid coated with carbon. Prior to analysis using HR-TEM (Tecnai G2 20 TWIM, FEI Pvt. Ltd., USA), all samples underwent sonication for 15 minutes and were left to dry under vacuum overnight (154).

4.5.4.2 Atomic force microscopy (AFM) analysis

AFM imaging of ASA-ALB-NPs and CTX-ASA-ALB-NPs was performed using Scanning Probe Microscopy (SPM) equipment, specifically the INTEGRA Prima system from NT-MDT Service and Logistics Ltd. The prepared ALB-NPs were appropriately diluted with HPLC-grade water and then subjected to 10 minutes of sonication in a bath sonicator. Before AFM analysis, a drop of each ASA-ALB-NPs and CTX-ASA-ALB-NPs suspension was placed on separate glass slides (2 x 2 cm) and dried under vacuum for 12 hours. The NOVA software provided by NT-MDT was utilized to capture both 2-D and 3-D AFM images of the ALB nanoparticles (155).

4.5.5 Surface chemistry (XPS) analysis

X-ray photoelectron spectroscopy (XPS) was employed to analyze the elements present on the surface of ASA-ALB-NPs and CTX-ASA-ALB-NPs. The analysis was conducted using a K-Alpha system by Thermo Fisher Scientific, USA, within the binding energy range of 100 to 800 electron volts (eV). Prior to XPS analysis, a concentrated suspension of nanoparticles was applied to a glass slide measuring 1 × 1 cm. The sample was subsequently vacuum-dried overnight (183).

4.5.6 Assessment of entrapment efficiency

The entrapment efficiency (EE) of both ASA-ALB-NPs and CTX-ASA-ALB-NPs was assessed through HPLC analysis using an LC-20AR Shimadzu system from Tokyo, Japan.
In summary, approximately 0.2 mL of the NPs suspension containing around 60 µg of ASA was evaporated in a round-bottom flask. Methanol was then introduced to the dried NPs residue and thoroughly mixed. The resulting mixture was centrifuged at 4500 rpm for 20 minutes, and the obtained supernatant was further evaporated using a rotary evaporator. An HPLC method was established employing a mobile phase consisting of a 50:50 methanol/water ratio. A standard curve for ASA was constructed based on peak area and concentrations (ranging from 100 to 1000 ng), showing a nearly linear curve with a regression coefficient of $R^2 = 0.998$. The percentage of drug encapsulated within the NPs formulations was determined by calculating the ratio between the amount of ASA loaded and the initial amount of ASA added to the NPs. NPs.

$$EE\%(w/w) = \frac{Amount\ of\ asiatic\ acid\ entrapped\ within\ nanoparticles}{Total\ amount\ of\ asiatic\ acid\ added\ to\ the\ formulation} \times 100$$

The previously mentioned approach was applied to assess the entrapment efficiency (EE) of C6-loaded ALB-NPs, both targeted and non-targeted. The C6 content in different NPs was quantified using a microplate reader operating in fluorescence mode. In summary, 3 mL of the

NP suspension was evaporated using a rotary evaporator. The dried C6 content was mixed with 70 µL of ethanol, and this mixture was then combined with 1 mL of distilled water. The resulting solution was filtered using a 0.22 µm filter. To determine the amount of free C6, the filtered solution was analyzed using a multimodal plate reader (Molecular Devices, SpectraMax M series, USA) with excitation and emission wavelengths of 457 nm and 502 nm, respectively. The provided equation was employed to calculate the percentage of C6 entrapment efficiency (172).

4.5.7 Thermal analysis of ALB-NPs

4.5.7.1 Differential Scanning Calorimetry (DSC) analysis

We explored the thermal compatibility among ALB, TPGS, and ASA using the DSC-60 Plus instrument (Shimadzu Asia Pacific Pvt. Ltd.). The analysis aimed to assess the thermal characteristics and interactions among these substances at varying temperatures. In summary, ASA, ALB, TPGS, a physical mixture of ASA and ALB, lyophilized ASA-ALB-NPs, and CTX-ASA-ALB-NPs were placed in a standard aluminum pan. The analyses were conducted with a heating rate of 10 ºC/min. and temperature ranges from 25 ºC to 400 ºC. An empty aluminum pan was used as a reference baseline. This study aimed to provide insights into the thermal properties of the samples and enhance our understanding of their behavior under different heating conditions (159).

4.5.7.2 Thermogravimetric Analysis (TGA) analysis

The thermal stability of ALB, ASA, TPGS, ASA-ALB-NPs, and CTX-ASA-ALB-NPs was estimated by using TGA-50 (M/s Shimadzu Asia Pacific Pvt Ltd., Japan). To investigate the thermal characteristics of the samples, they were exposed to a gradual rise in temperature ranging from 25 ºC to 800 ºC, with a heating rate of 10 ºC/min. Additionally, a steady flow of dry nitrogen was introduced at a rate of 100 mL/min to maintain a controlled environment during the heating process (160).

4.6 *In vitro* studies

4.6.1 *In vitro* drug release study

The *in vitro* release of ASA from the prepared NPs was quantified using the dialysis bag technique, which mimicked both normal cell conditions (using PBS at pH 7.4) and cancerous cell conditions (using sodium acetate buffer at pH 5.0). Specifically, 0.3 mg of ASA-ALB-NPs and CTX-ASA-ALB-NPs were placed in separate dialysis bags with a molecular weight cutoff of 1 kDa and sealed securely. These dialysis bags were immersed individually in vessels containing 50 mL of either PBS at pH 7.4 or acetate buffer at pH 5.5. The solutions were continuously stirred at 37 ± 0.5 ºC on a magnetic stirrer set at 100 rpm. At specific time intervals, 2 mL of the sample solution was withdrawn, and 2 mL of fresh buffer solution was added to maintain a consistent volume and ensure sink conditions. The samples were then processed and analyzed using HPLC. After determining the ASA concentration in each sample, a graph illustrating cumulative drug release over time was generated (43).

4.6.2 Cell line maintenance and cell culture growth conditions

The A549 cell line (human lung adenocarcinoma) and HEK 293 cell line (normal human embryonic kidney) were used in the study. These cell lines were cultured in Dulbecco's Modified Eagle Medium (DMEM) containing 10 % fetal bovine serum (FBS), 100 IU/mL penicillin, streptomycin, and 1 % amphotericin B solution. The cells were maintained in a humidified carbon dioxide incubator at 37 ºC under 5 % CO_2 and 95 % relative humidity. For the preparation of single-cell suspension, cells were cultured in monolayers and treated with 0.25 % (w/v) trypsin/EDTA (1 mM).

4.6.3 Cell cytotoxicity study

To assess the potential cytotoxicity of pure ASA, ASA-ALB-NPs, and CTX-ASA-ALB-NPs, an MTT assay was performed using A549 (lung cancer cell line) and HEK-293 (normal cell line) cells. Standard docetaxel was utilized as a control (163). Cells were seeded at a density

of 1×10^4 viable cells per well in 96-well plates containing DMEM and incubated at 37 ºC under a 5% CO_2 humidified atmosphere for 24 hours. After the initial incubation, the cells were treated with varying concentrations (0.1, 1, 10, and 100 µg/mL) of pure ASA, ASA-ALB-NPs, CTX-ASA-ALB-NPs, and standard docetaxel for 24 hours in a dose-dependent manner (in triplicate).

After the treatment period, 10 µL of MTT solution (5 mg/mL in PBS at pH 7.4) and 100 µL of fresh media were added to the wells of the microplate. Subsequently, the microplates were incubated for an additional 4 hours. Following this incubation, 100 µL of DMSO was introduced to each well to dissolve the formazan crystals. The optical density (OD) of the samples was measured at a wavelength of 570 nm using a microplate reader (Synergy H1 Hybrid Multimode Microplate Reader, BioTek, USA).

To determine cell viability, the absorbance of treated cells was measured and compared to that of untreated cells (44). The study was conducted in triplicate to ensure the accuracy and reliability of the results. The calculation of cell viability percentage was performed using the following formula:

$$Cell\ viability\ (\%) = \frac{Absorbance\ of\ treated\ cells}{Absorbance\ of\ control\ cells}\ \text{x}\ 100$$

4.6.4 Cellular uptake of ALB-NPs

Cells numbering 5×10^4 per well were placed in 12-well plates and allowed to incubate for 24 hours. Afterward, both free and C6-loaded formulations, each at a concentration of 5 µg/mL, were added to the wells and incubated at 37 ºC for 12 hours. The cells were then washed three times with 1x PBS and permeabilized using Triton X-100. Following this, the cells were fixed with a 4% formaldehyde solution for 15 minutes and stained with 4′,6-diamidino-2-phenylindole (DAPI) to label the nuclei. After removing the DAPI-containing medium, the cells were washed with PBS. Fluorescent images of the treated cells were captured using

excitation wavelengths of 340 nm for the blue channel (DAPI) and 488 nm for the green channel (C6). The percentage area of the green channels in A549 cells was quantified using Image-J software to assess the cellular uptake of nanoparticles (NPs) (45).

4.6.5 Apoptosis assay through acridine orange/ethidium bromide dual staining

The evaluation of cytotoxicity induced by nanoparticle formulations on A549 cells involved an examination of cell morphology. Variations in the treated cells' appearance were observed using an inverted fluorescent microscope. Apoptosis, a natural process vital in multicellular organism development, was studied. A dual staining approach, employing acridine orange (AO) and ethidium bromide (EB), was used to distinguish between live and dead cells based on their membrane integrity (46). Changes in cell morphology and chromatin structure enabled the differentiation between necrotic and apoptotic cells (47). Acridine orange (AO) could permeate the plasma membrane of both live and dead cells, emitting green fluorescence upon binding to viable cell nuclei. In contrast, ethidium bromide (EB) exclusively stained the DNA of dead cells with compromised membrane integrity, displaying a red-orange fluorescence.

In brief, A549 cells were initially seeded at a density of (1×10^5) cells per well in 12-well tissue culture plates and cultured for 24 hours in a 5 % CO_2 environment. Subsequently, these A549 cells were exposed to ASA, ASA-ALB-NPs, and CTX-ASA-ALB-NPs at a concentration equivalent to the IC_{50} value (11.6 µg/mL) for 24 hours, maintained in a CO_2 incubator. Afterward, the cells were rinsed with PBS 7.4 and then stained with AO and EB solutions (40 µg/mL), followed by an incubation at 37 ºC for 25 minutes. Following the treatment, the cells were washed with PBS and examined for any morphological alterations using a fluorescent microscope (Nikon Inverted Microscope Eclipse Ti-U) equipped with both red and green channels (48).

4.6.6 AnnexinV-Alexa Fluor 488/Propidium iodide staining assay

The assay facilitates the detection of various stages and types of cell death. The A549 cells were subjected to Annexin V-Alexa Fluor 488 and Propidium Iodide (PI) staining to quantify the proportion of apoptotic cells via flow cytometry, utilizing Invitrogen™ Dead Cell Apoptosis Kits (ThermoFisher Scientific) (49).

A549 cells were seeded at a density of 1×10^5 cells per well in a 6-well culture plate and incubated for 24 h. Subsequently, the cells were exposed to ASA, ASA-ALB-NPs, and CTX-ASA-ALB-NPs at a concentration of 11.6 µg/mL for 24 h. Following the incubation period, the cells were collected and washed with cold PBS, centrifuged, and then suspended in 1x annexin-binding buffer. In this study, Annexin V-Alexa Fluor solution (5 µL) and PI solution (100 µg/mL working solution) were added consecutively to 100 µL of cell suspension. Next, cells were incubated in the dark at room temperature for 20 min. The cells were then mixed with 1X annexin-binding buffer and kept on ice. Cell apoptosis was analyzed using flow cytometry (BD FACS Calibur, USA), and the data were presented as a dot plot of Annexin V-Alexa fluor versus PI with quadrant gating.

4.6.7 Cell cycle analysis

The purpose of this research was to examine how exposure to ALB-NPs affects the distribution of cell cycle phases. The cell cycle comprises four distinct stages: the Gap1 phase, the DNA synthesis phase, the Gap2 phase, and the Mitosis phase. One approach to cancer treatment involves halting the cell cycle at a specific phase using anti-cancer drugs.

Briefly, A549 cells were initially placed in a six-well plate with a concentration of 1×10^5 cells per well and incubated for 24 hours. Subsequently, the cells were treated with 11.6 µg/mL of ASA-ALB-NPs and CTX-ASA-ALB-NPs for 24 hours. After the treatment, the cells were trypsinized, washed with chilled PBS, and centrifuged at 1000 rpm for 5 minutes.

The suspended cells in cold PBS were fixed using 70 % v/v ethanol at 4 ºC. Following fixation, the cells were washed with PBS and maintained at 4 ºC. Then, the cells were exposed to RNase (40 µg/mL) in a buffer containing 0.1 % sodium citrate and kept at 37 ºC for 30 minutes. Later, the cells were stained with a buffer containing propidium iodide (50 µg/mL), a red fluorescent dye, in the presence of 0.03 % Triton X-100 and 0.1 % sodium citrate for 30 minutes at 37 ºC in the dark.

Using a BD FACS Verse flow cytometer, 10,000 events were recorded for each sample in the PI channel. During analysis, an appropriate gate was applied to exclude doublets and aggregates. Following incubation, each sample was analyzed using a BD FACS Calibur flow cytometer to identify alterations in the distribution of cell cycle phases.

4.6.8 Pharmacokinetic study

The study involved the use of healthy Wistar rats, aged 5-6 weeks and weighing between 180-220 grams. These rats were obtained and placed in a controlled environment with a temperature maintained at 25 ± 2 ºC and controlled humidity, following a 12-hour light/dark cycle. A 15-day acclimatization period was allowed for the rats, during which they had unrestricted access to food. A total of sixteen Wistar rats were randomly divided into four groups, which included the Saline control group, ASA control group, ASA-ALB-NPs group, and CTX-ASA-ALB-NPs group. In this study, the saline control group received only saline, while the ASA control group and the two experimental groups were given a 10 mg/kg dose of ASA and various formulations of ALB-NPs through intravenous administration via the tail vein.

Blood samples were obtained from each group of rats at specific time intervals (0.5, 1, 2, 4, 8, 12, and 24 hours) via the retro-orbital venous plexus. These samples were collected in microcentrifuge tubes containing 3.8% sodium citrate and stored for later analysis. Subsequently, the collected samples underwent centrifugation at 4,000 rpm for 15 minutes to separate the plasma. After plasma separation, 200 µL of the resulting clear plasma was mixed

with a mobile phase composed of a 50:50 mixture of methanol and water. The mixture was vortexed for 5 minutes and then centrifuged for 15 minutes at 3,500 rpm. The resulting clear supernatant was transferred to HPLC vials.

To assess the ASA content in plasma-derived samples, RP-HPLC with an ODS C18 column (250 mm x 4.6 mm, 5 μm) was used. A PDA detector (SPD-M40 PDA detector 1 with 1024 diodes) was employed to monitor the samples at a wavelength of 206 nm. For analysis, a 10 μL portion of each sample was injected into the HPLC column, and the resulting data was compared to a standard calibration curve. To determine the pharmacokinetic parameters of ASA in various ALB formulations, a graph was created by plotting the drug concentration in plasma against time (49,50). The data obtained through RP-HPLC were examined for their pharmacokinetic implications using Kinetic 5.0 software, which is provided by Thermo Fisher Scientific.

4.6.9 Histopathology

The current study utilized histopathological examination to assess the harmful effects and mortality linked to the administration of ASA, as well as non-targeted and targeted ALB-NPs. Experimental animals were divided randomly into four groups, each comprising four rats.

The experimental animals were treated with the saline control, ASA, ASA-ALB-NPs, and CTX-ASA-ALB-NPs formulations at a dosage of 10 mg/kg via intravenous injection (through the tail vein) once every three days for a total of three treatments (on the 1st, 3rd, 6th, and 9th day). On the 15th day of the experiment, the animals were euthanized, and vital organs such as the heart, kidneys, liver, and lungs were removed and cleaned with distilled water. The tissue samples were fixed in 10% formalin and then embedded in paraffin. These paraffin-embedded samples were cut into 5 μm thick sections using a microtome. Subsequently, the sections were stained with haematoxylin and eosin, and histopathological assessments were conducted by capturing images with a brightfield microscope (Dewinter microscope).

4.7 Statistical analysis

Statistical analysis was conducted on the data obtained from a minimum of three independent experiments using GraphPad PRISM® Version 5.01 software (GraphPad, USA). To compare data between two groups, an unpaired Student's t-test was utilized, while one-way ANOVA (analysis of variance), along with Tukey's post hoc test, was used for multiple groups. The data are reported as mean ± standard error of the mean. The significance level was assigned and is represented by the following notation: ns (non-significant) for $p \geq 0.05$, * for $p < 0.05$, ** for $p < 0.01$, and *** for $p < 0.001$ are representing significant levels.

4.8 Results and discussion

4.8.1 *In silico* docking

In silico docking studies were performed to explore the compatibility of different biodegradable proteins with ASA (Table 10). Three biodegradable proteins: bovine serum albumin (PDBID:4JK4), bovine beta-lactoglobulin (PDBID:3NPO), and bovine lactoferrin (PDBID:1BLF) were chosen as carriers. Fig. 30 represents the lowest binding affinities of different proteins with ASA, based on the various types of interactions between ASA and protein carriers. Comparing the values of the binding energies, the binding affinity of albumin and ASA is predicted to be stronger, about -7.9 kcal/mol, which is the lowest among -7.4 kcal/mol (3NPO) and -6.5 kcal/mol (1BLF) all theoretically tested polymers. 2D interaction of ligand (ASA) with the protein 4JK4 revealed that the methyl group of ligand undergoes alkyl-alkyl interaction with ILE297, LEU301, PRO303, LEU304, and PHE373 residues. Similarly, the cyclohexane ring also formed alkyl-alkyl interaction with ARG336 residue. In addition, the hydroxyl group of Asiatic acid exhibited conventional hydrogen bond interaction with GLU299 and LEU301 residues, respectively.

Table 10 Docking interaction between ligand (ASA) and proteins: binding energies and interacting amino acids

Ligand	Protein	Binding Energy (kcal/mol)	Interacting Amino acids
ASA	4JK4	-7.9	GLU299, ASN300, LEU301, PRO302, ARG336, PRO303, THR305, LEU304, PHE373, TYR333, HIS337, ILE297
ASA	3NPO	-7.4	LYS69, PRO38, GLU114, ASN109, ASN88, SER116, LEU31, LEU39, ALA86, ASN90, ILE84, ILE71
ASA	1BLF	-6.5	GLU664, ALA668, ASN671, LEU473, ASN476, LEU672, GLY472, ASN468, ILE469, ALA590, TYR665, VAL591

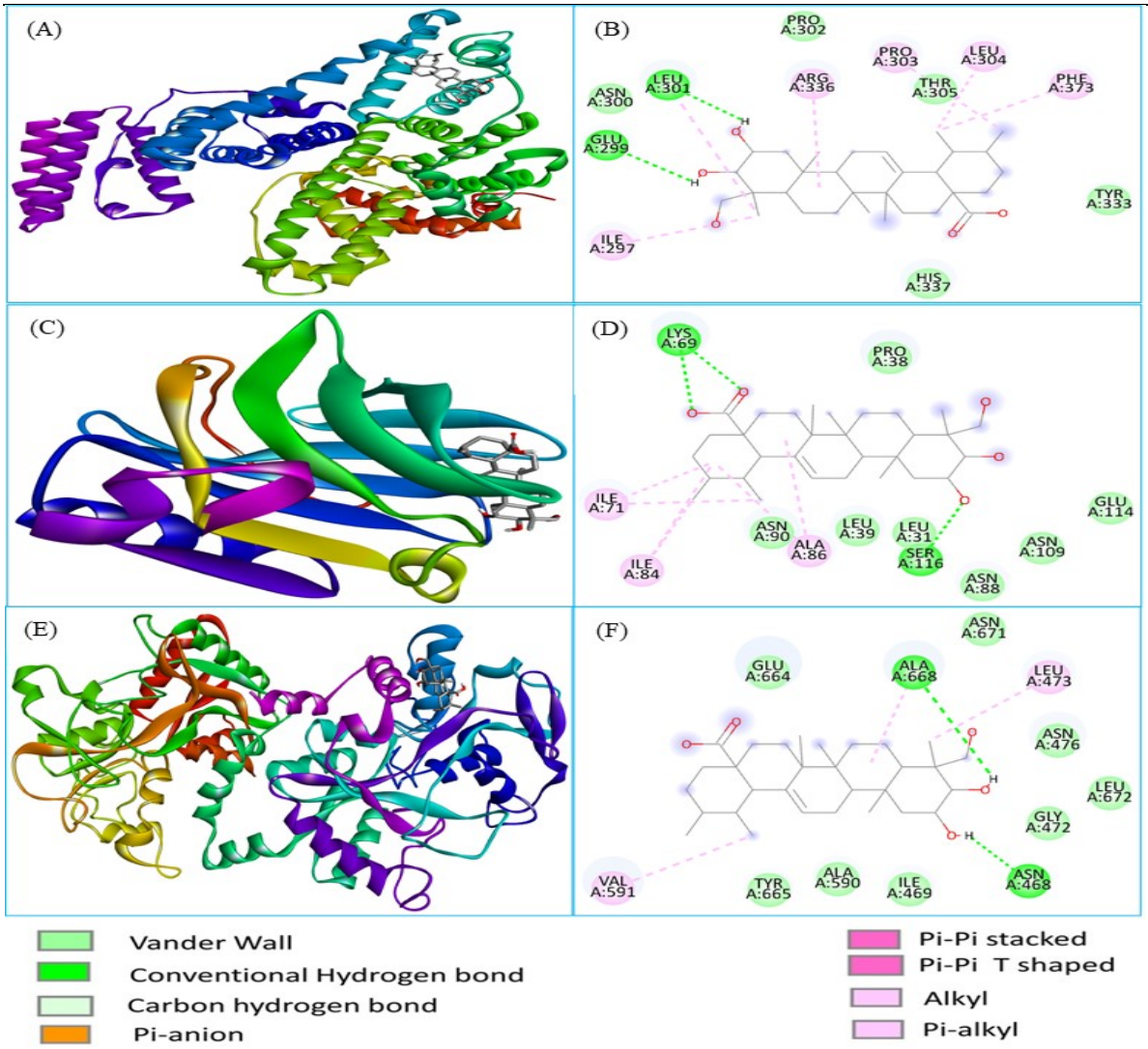

Figure 30 3D (A) and 2D (B) binding interaction of ASA against bovine serum albumin (4JK4); 3D (C) and 2D (D) binding interaction of ASA against bovine beta lactoglobulin (3NPO); 3D (E) and 2D (F) binding interaction of ASA against bovine lactoferrin (1BLF) respectively

4.8.2 Characterization of TPGS-SA

The HRMS spectra of TPGS and TPGS-SA show that various oligomeric conformations with different adduct and charge states have been explored (184). The molecular formula of TPGS that formed a sodium adduct was confirmed to be $C_{33}H_{54}O_5$-$(CH_2CH_2O)_n$ + Na. The HRMS analysis of TPGS-SA revealed an increase of 101 Da in the mass of multiple oligomers, indicating a reaction between TPGS and succinic anhydride. This increase in mass corresponds to the molecular weight of succinic anhydride, providing strong evidence for the occurrence of the TPGS-succinic anhydride reaction. An expected empirical formula for various oligomers of TPGS-SA forming sodium adduct could be $[C_{33}H_{54}O_5$-$(CH_2CH_2O)_n]$-CO-C_2H_4-COOH + Na (184). Additionally, the spectra of TPGS and TPGS-SA reveal the presence of oligomers in various charge states. For example, the oligomer of TPGS with an n value of 20, $[C_{33}H_{54}O_5$-$(CH_2CH_2O)]_{20}$, with a molecular weight of 1410 Da (or m/z 1433 in the form of sodium salt), undergoes a reaction with succinic acid resulting in a species with m/z 1534 (184). By comparing the spectra of TPGS and TPGS-SA, similar kinds of increments were noticed. Furthermore, in the mass spectrum analysis of TPGS, several peaks were observed at m/z values of 1477, 1521, 1565, 1609, and 1653. Correspondingly, comparable peaks (with a 101-unit increase) were detected in the mass spectrum of TPGS-SA at m/z 1578, 1622, 1666, 1710, and 1754, respectively (184). The confirmation of the TPGS-SA structure was further validated through the analysis of its ^{1}H NMR spectra. The resulting ^{1}H NMR spectrum of TPGS-SA indicated the detection of signals corresponding to the ethylene protons of PEG at a range of δ 3.5-3.6. The aliphatic region (δ 1-3) of spectra contains signals corresponding to the various protons in the vitamin E-tail. The ^{1}H NMR spectra of TPGS-SA revealed comparable signals to those observed in the TPGS spectra, with the exception of the succinyl methylene (-CH_2) protons at δ 3.0 and 2.3 ppm. This observation confirmed that a chemical reaction had taken

place between TPGS and succinic anhydride (184). The TPGS-SA spectral data were matched with the reported literature and was found suitable.

4.9 NPs characterization

4.9.1 Size, polydispersity, and zeta potential of NPs

Table 11 presents the physicochemical assessment characteristics of ALB-NPs. The resulting formulations displayed hydrodynamic diameters that were below 200 nm. Incorporation of the ligand (CTX) onto the surfaces of nanoparticles led to an increase in particle size ($p < 0.05$). The zeta potential of ASA-ALB-NPs was -26.7 ± 3.5 mV, which was reduced to -29.5 ± 4.6 mV following conjugation with cetuximab in CTX-ASA-ALB-NPs. This could be attributed to the existence of the prevailing anionic groups in the structure of CTX, which rendered a more negative surface charge to CTX-ASA-ALB-NPs. As per the literature, we have observed that the most stable range of the zeta potential of the NPs was observed to be + 40 mV to - 40 mV, and our developed NPs were within this range.

Table 11 Particle size, Polydispersity-index, zeta-potential, and entrapment efficiency of ALB-NPs.

Batches	Particle size (nm)	Polydispersity index	Zeta potential (mV)	Entrapment efficiency (%)
ASA-ALB-NPs	178.5 ± 3.3	0.24 ± 0.02	-26.7 ± 3.5	71.3 ± 5.7
CTX-ASA-ALB-NPs	183.2 ± 2.8	0.28 ± 0.07	-29.5 ± 4.6	68.8 ± 4.7
C6-ALB-NPs	177.6 ± 4.4	0.25 ± 0.05	-28.6 ± 3.1	72.5 ± 3.8
CTX-C6-ALB-NPs	186.3 ± 2.9	0.32 ± 0.06	-31.45 ± 3.3	70.6± 4.1

**** Each data was represented as a mean ± standard deviation (n=3)***
ASA-ALB-NPs: Asiatic acid-loaded ALB-NPs.
CTX-ASA-ALB-NPs: Asiatic acid loaded CTX conjugated ALB-NPs.
C6-ALB-NPs: Coumarin-6 loaded ALB-NPs.
CTX-C6-ALB-NPs: Coumarin-6 loaded CTX conjugated ALB-NPs.

4.9.2 FTIR spectroscopy

The FTIR analysis of ALB revealed the presence of a peak at 3312 cm^{-1}, which was assigned to the NH stretching of the primary amine group of the protein. Additionally, three distinct vibrational bands at 1659, 1537, and 1241 cm^{-1} were observed, which were attributed to the amide linkages of bovine serum albumin (ALB). The characteristic peaks in the ASA spectrum were found at 3407 cm^{-1} (O-H Stretching), 2925 cm^{-1} for (C-H stretch), and 1690 cm^{-1} for C=O stretching vibrations (Fig. 31A). Peaks of ASA and ALB were less prominent in ASA-ALB-NPs, and CTX-ASA-ALB-NPs in comparison to the physical mixture (ALB + ASA), which reflect the successful interaction of ingredients in ALB-NPs. Table 12 depicts the FTIR spectra data of ASA, ALB, physical mixture of ASA, CTX, ASA-ALB-NPs, and CTX-ASA-ALB-NPs (50, 51).

Table 12 FTIR peak assignment of ALB, ASA, TPGS, CTX, ASA-ALB-NPs, CTX-ASA-ALB-NPs

S.No.	Types of stretching & bending vibration	Characteristic absorption bands / peaks ν_{max} cm^{-1}					
		ALB	**ASA**	**TPGS**	**CTX**	**ASA-ALB-NPs**	**CTX-ASA-ALB-NPs**
1.	O-H Stretching	-	3407 cm^{-1}	3465 cm^{-1}	3435 cm^{-1}	3435 cm^{-1}	3848 cm^{-1} 3743 cm^{-1}
2.	N-H Stretching	3312 cm^{-1} 3057 cm^{-1}	-	-	-	-	3446 cm^{-1}
3.	C-H Stretching	2944 cm^{-1}	2925 cm^{-1}	2886 cm^{-1}	2757 cm^{-1}	2914 cm^{-1}	2916 cm^{-1}
4.	C=O stretching	1659 cm^{-1}	1690 cm^{-1}	1741 cm^{-1} 1618 cm^{-1}	1629 cm^{-1}	1639 cm^{-1}	1641 cm^{-1}
5.	C–N stretching	1241 cm^{-1}	NA	NA	1238 cm^{-1}	1243 cm^{-1}	1249 cm^{-1}
6.	N–H bending	1537 cm^{-1}	NA	-	1532 cm^{-1}	1516 cm^{-1}	1541 cm^{-1}

7.	C-O stretching	1088 cm^{-1}	1050 cm^{-1}	1074 cm^{-1}	1057 cm^{-1}	1047 cm^{-1}	1057 cm^{-1}

4.9.3 XRD analysis

Fig. 31B shows the XRD overlay spectrum of ASA, ALB, ASA-ALB-NPs, and CTX-ASA-ALB-NPs. XRD spectrum of pure ASA exhibited strong, sharp peaks at 16.43º and 24.34º, indicating the crystalline state. Whereas the XRD spectrum of TPGS displayed two sharp characteristic peaks at 19.07º, and 23.15º and also consisting of broad peaks (26.20 and 35.92º), revealing its semi-crystalline nature. The ALB spectrum shows broad peaks at approx. 20.59° demonstrated its amorphous nature. However, the ASA-ALB-NPs and CTX-ASA-ALB-NPs consist of two single sharp peaks with intensity at 2θ of 24.17º and 28.26º, displaying their semicrystalline state. However, these peaks were less intense in the CTX-conjugated NPs as compared to non-targeted NPs, which may be due to the presence of CTX.

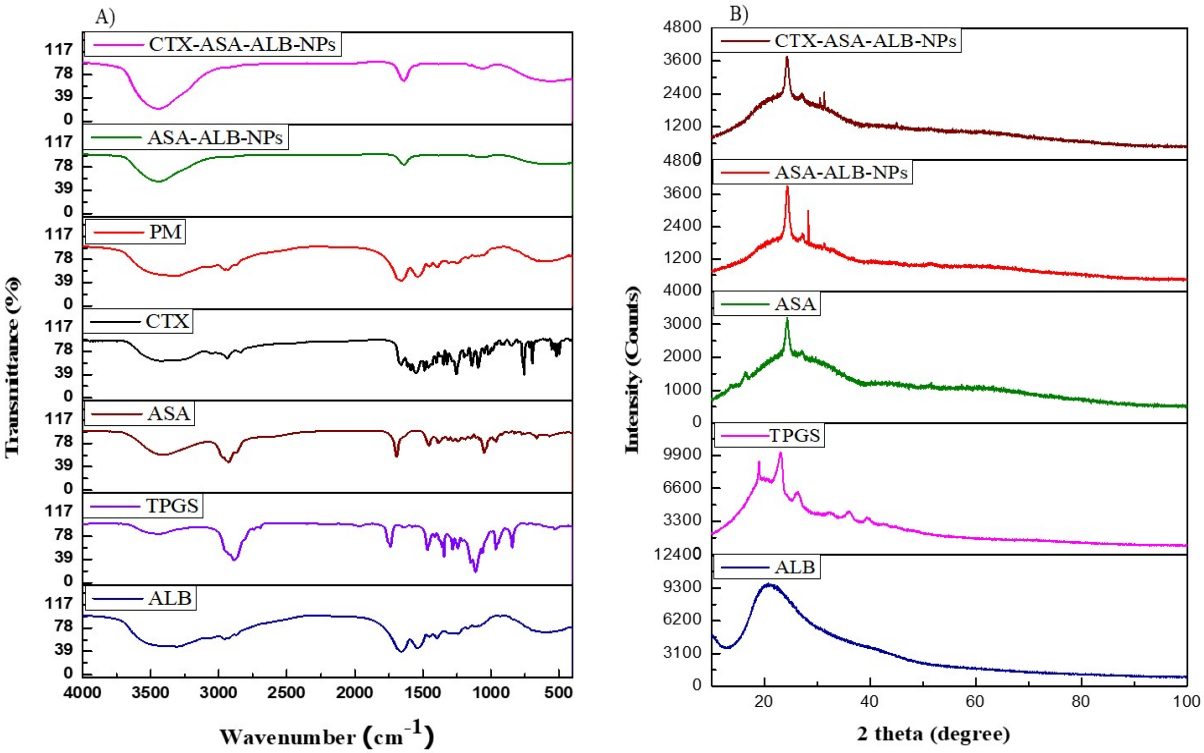

Figure 31 A) FTIR analysis of drug, excipients, physical mixture, non-targeted and CTX conjugated ALB-NPs. B) XRD analysis of ALB, TPGS, ASA and non-targeted and CTX conjugated ALB-NPs.

4.9.4 Morphological Assessment of ALB-NPs

4.9.4.1 TEM

The shape, morphology, size, and physical state of the ALB-NPs were examined using TEM. TEM images of NPs at 200 nm scale are shown in Fig. 32A. Individual particles appear spherical and evenly distributed.

4.9.4.2 AFM

The surface topology and morphology of ALB-NPs were investigated using AFM analysis. The NPs were smooth-surfaced and spherical, as seen by the 2-D and 3-D AFM images in Fig. 32B and 32C, with no obvious pinholes or cracks.

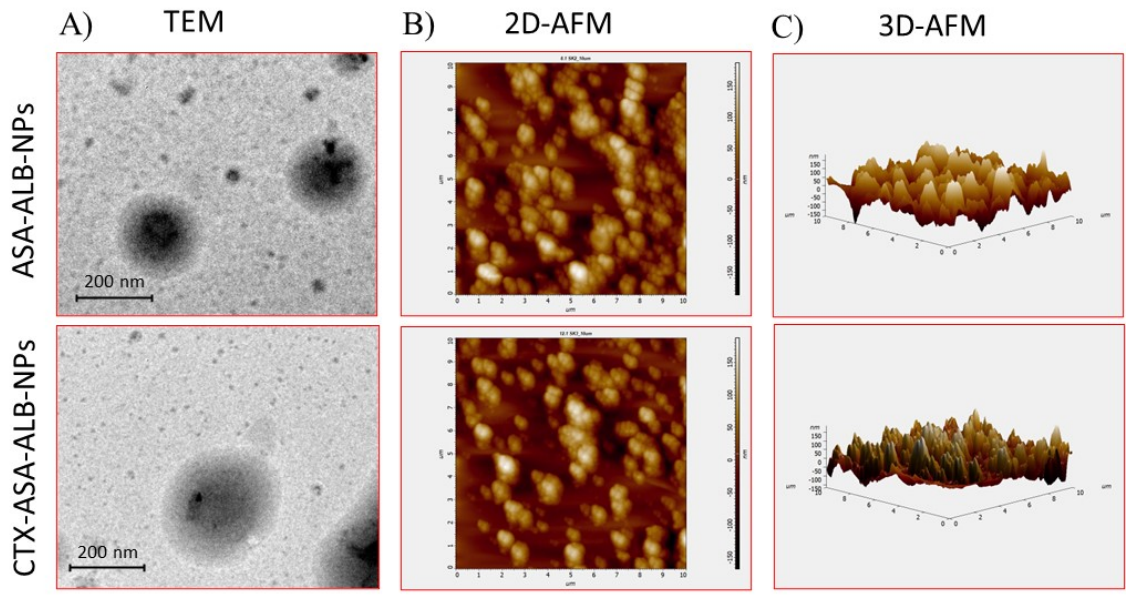

Figure 32 Morphological analyses of non-targeted and CTX conjugated ALB-NPs.

4.9.4.3 XPS analysis

Nanoparticles, including non-targeted (ASA-ALB-NPs) and targeted formulations (CTX-ASA-ALB-NPs), were analyzed using the XPS technique to determine their surface chemistry. Fig 33A. shows the expected peaks for elements such as carbon, nitrogen, and oxygen from the acquired XPS spectra. Peaks observed at binding energies of 290-280 eV, 404-395 eV, and

537-527 eV were attributed to C 1s, N 1s, and O 1s, respectively. In the XPS survey of non-targeted and CTX-conjugated NPs, the atomic percentage of nitrogen atoms was 1.19 ± 0.56 and 5.11 ± 0.81, respectively, depicting that the atomic percentage of N 1 s was about 4 folds higher ($p < 0.001$) in the CTX conjugated ALB-NPs (Fig 33B). ALB-NPs successfully conjugated with CTX are supported by the enhanced nitrogen percentage in the XPS spectra of CTX-ASA-ALB-NPs, which can be attributed to a large number of nitrogen atoms present in CTX (52).

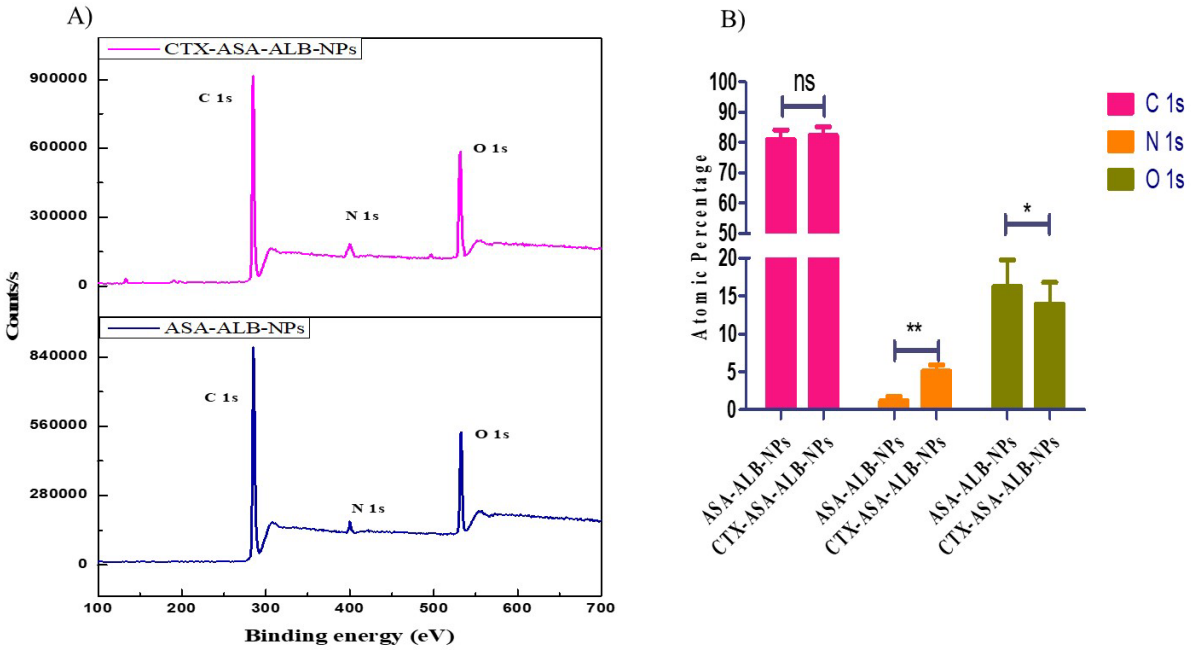

Figure 33 XPS analysis of non-targeted and CTX conjugated ALB-NPs. B) Histogram showing atomic percentage on the nanoparticle surface

4.9.5 DSC analysis

The thermal properties of ASA in NPs were assessed using the DSC analyzer. This instrument measures the heat flow of a sample across a range of temperatures, making it well-suited for evaluating the thermal behaviour of the ASA in NPs (185). Fig. 34A shows the thermograms of ASA, ALB, physical mixture of ASA and ALB, ASA-ALB-NPs, and CTX-ASA-ALB-NPs. The DSC curve of ALB showed characteristic endothermic peaks at 62.1 ºC, 218.4 ºC, 285.8 ºC, 310.1 ºC, 323.4 ºC, 345.2 ºC. The ALB endothermic peak at 62.1 ºC, indicates melting of

the ALB, other peaks indicate the phase transition and degradation of the ALB. Whereas DSC curves of TPGS showed sharp endotherm at 39.6 ºC, indicating its melting point. The DSC curve of ASA exhibited a sharp endotherm at 331.9 ºC, revealing its melting point. However, a small exothermic peak was also observed at 249.9 ºC. The physical mixture of ASA and ALB showed a small endotherm related to the ASA at the same temperature, which showed no chemical interaction. The non-targeted NPs displayed peaks at 50.7 ºC and 224.1 ºC and demonstrated good thermal stability. Whereas the CTX-targeted NPs exhibited several endothermic peaks at 56.5 ºC, 220.4 ºC, and 308.5 ºC. Since the endothermic peak of ASA was missing in both of the NP's formulations, it supports its appropriate entrapment in the ALB matrix and, therefore, improves its thermal stability.

4.9.6 TGA analysis

Thermogravimetric analysis (TGA) was used to measure percent weight changes of ALB, ASA, TPGS, physical mixture, and ALB-NPs as a function of temperature, which demonstrated their thermal stability and undesired physical or chemical interactions.

Fig. 34B, shows the temperature stability and the degradation of ALB-NPs with respect to increasing temperature. The results depicted that there was no significant weight loss of ALB and physical mixture up to 200 ºC. Moreover, the TGA curve of TPGS and ASA showed considerable weight loss (approximately 90 %) between 300 ºC to 400 ºC indicating a faster rate of degradation and lesser thermal stability above 300 ºC. However, the TGA curve of the physical mixture of ALB and ASA exhibited 58 % weight loss between 300 ºC to 400 ºC indicating slow degradation than ASA alone, which was also confirmed with DSC curve. Contrastingly, ASA-ALB-NPs and CTX-ASA-ALB-NPs, showed a lesser percentage of weight loss (around 49 % and 54 %, respectively), between 300 ºC to 450 ºC indicating their slower degradation rate indicating their improved stability compared to ASA.

The TGA curve of TPGS and ASA demonstrated rapid weight loss between 300 to 450 ºC, whereas both the NPs demonstrated slower degradation.

The findings unambiguously demonstrated that incorporating ASA into ASA-ALB-NPs and CTX-ASA-ALB-NPs enhanced its stability as compared to the standard ASA. Furthermore, the temperature stability analysis indicated that the products were effectively decomposed at elevated temperatures.

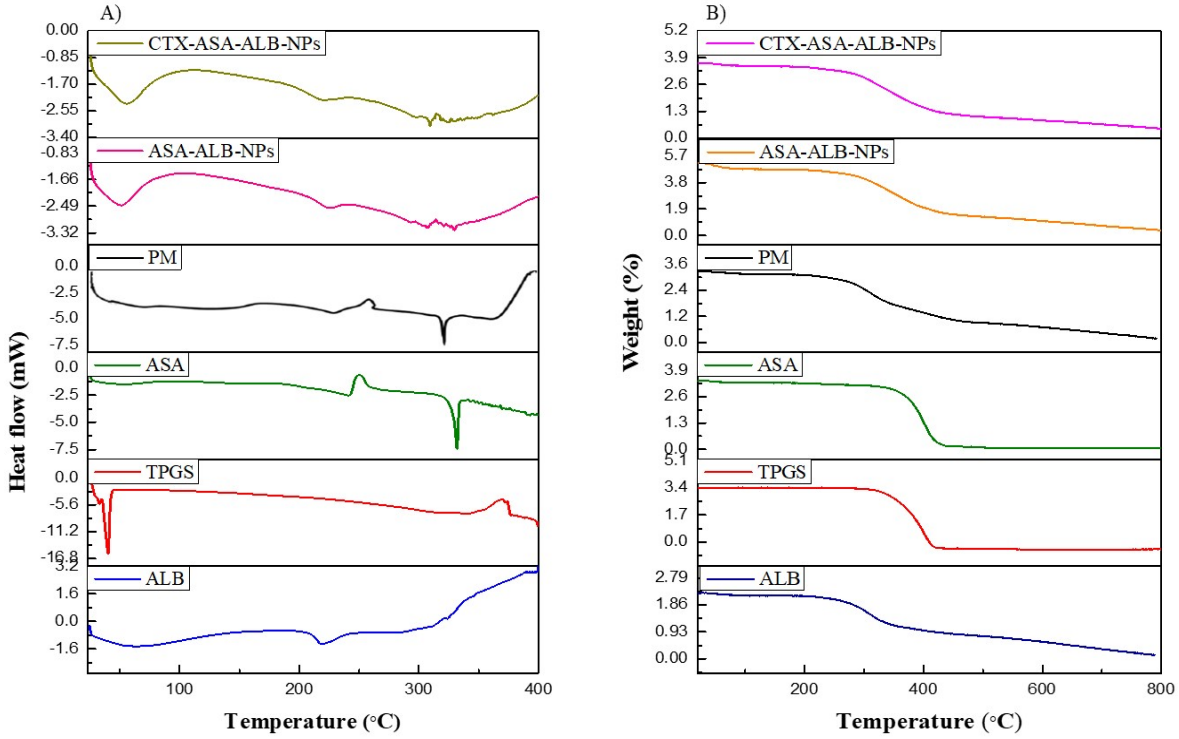

Figure 34 Thermal analysis A) DSC and B) TGA analysis of drug, polymer, excipients, physical mixture, non-targeted ALB NPs and CTX conjugated ALB NPs.

4.9.7 Entrapment Efficiency

The entrapment efficiency of ASA-ALB-NPs and CTX-ASA-ALB-NPs was 71.3 ± 5.7 % and 68.8 ± 4.7 %, respectively (Table 11). The small drop of the ASA content in targeted NPs may be due to the interference of the CTX conjugation on the surface.

4.10 *In vitro* analysis

4.10.1 *In vitro* release of drug from ALB formulations

The graph from the *in vitro* drug release analysis of the ASA-ALB-NPs and CTX-ASA-ALB-NPs (Fig. 35A) indicated an initial rapid release followed by a sustained release for up to 72 h. Furthermore, ASA release was higher in PBS pH 5.5, possibly due to albumin denaturation and precipitation, whereas it was comparably lesser in PBS 7.4. The outcomes showed that increased ASA release from ALB-NPs in a cancer microenvironment (pH 5.5.) may be advantageous for the targeted delivery of ASA.

4.10.2 Assessment of *in vitro* cytotoxicity

The MTT assay is a widely recognized colorimetric technique for determining cell viability that assesses the quantity of metabolically active cells by measuring the colour intensity generated from formazan formation after the reduction of MTT (54). This study assessed the cytotoxic impact of ASA, Docetaxel, and synthesized ALB-NPs on the A549 cell line. Additionally, treatments were administered to a normal cell line (HEK 293) to evaluate the specificity of the treatment and ensure its safety on normal cells. Fig. 35B depicts the results of the MTT assay after 24 h of treatment with ASA, Docetaxel, ASA-ALB-NPs, and CTX-ASA-ALB-NPs on A549 cells.

Fig. 35C illustrates the impact of ASA, Docetaxel, ASA-ALB-NPs, and CTX-ASA-ALB-NPs on normal (HEK 293) cells' cytotoxicity. After 24 h of treatment, the IC_{50} values of docetaxel (positive control), ASA control, ASA-ALB-NPs, and CTX-ASA-ALB-NPs were 25.3 ± 2.7 µg/mL, 106.34 ± 2.51 µg/mL, 31.59 ± 1.65 µg/mL, and 11.61 ± 1.58 µg/mL, respectively, in A549 cells. The IC_{50} value of CTX-ASA-ALB-NPs was about 2 folds ($p < 0.001$), 9 folds ($p < 0.001$), and 2.7 folds ($p < 0.001$) lesser than docetaxel, ASA control and ASA-ALB-NPs which indicates the cytotoxic nature of synthesized ALB-NPs against A549 cells.

Upon treatment with concentrations of 100 µg/mL of the developed nanoparticles (NPs) for 24 h in normal (HEK 293) cells, a viability rate of more than 70% was observed. This indicates that the developed NPs exhibit negligible cytotoxicity towards normal cells and can be deemed safe for such applications. The MTT assay demonstrated that CTX-ASA-ALB-NPs exhibit concentration-dependent cytotoxicity towards lung cancer cells (A549), leading to a significant reduction in cell viability. These findings suggest that CTX-ASA-ALB-NPs possess potent cytotoxic potential against lung cancer.

Furthermore, previous studies have demonstrated that ALB-NPs are safe and biocompatible for human consumption, as albumin is a naturally occurring protein in the human body. This supports the potential use of ALB-NPs as a safe and effective drug delivery system.

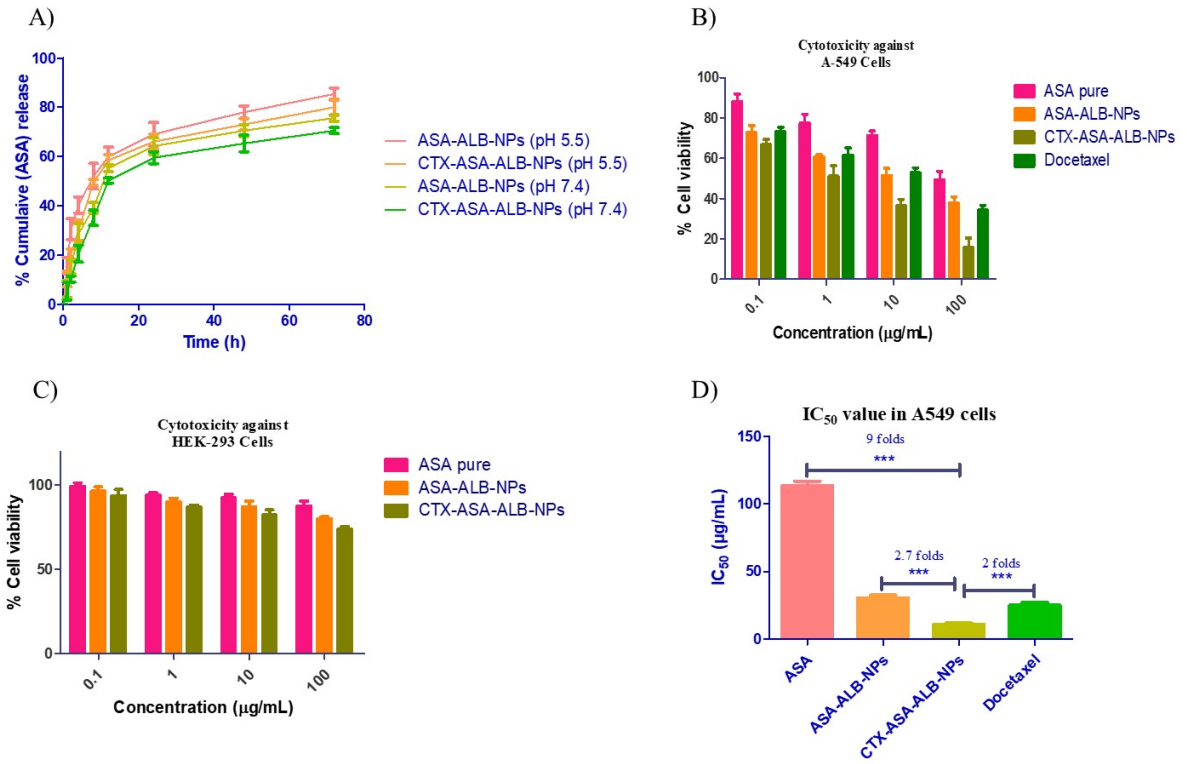

Figure 35 A) *In vitro* drug release profile in pH 5.5 and 7.4. B) Cell-viability analysis of ASA, ASA-ALB-NPs, CTX-ASA-ALB-NPs, and Docetaxel against A549 cancer cells and C) Cell-viability analysis of ASA, ASA-ALB-NPs, and CTX-ASA-ALB-NPs against HEK-293 cells. D) Statistical analysis among ASA, ASA-ALB-NPs, and CTX-ASA-ALB-NPs.

4.10.3 Investigation of *in vitro* cellular uptake

The green channel in Fig. 36A represents the degree of internalization of C6-loaded NPs. We measured the amount of green fluorescence using the image analysis program Image-J (Fig. 36B). The level of internalization was measured by determining the percentage area of green channels in the image. The histogram reveals that the percentage area of green channels in the fluorescence images of CTX-conjugated NPs was significantly higher compared to the C6 control ($p < 0.001$) and non-targeted NPs ($p < 0.001$), with a 27-fold and 5-fold increase, respectively. The findings implied that the enhanced uptake of CTX-conjugated NPs in A549 cells could be attributed to EGFR-mediated endocytosis. The main purpose of the cellular uptake study was to confirm the drug delivery mechanism to the cancer cells. The study demonstrated that targeted NPs were more efficiently uptaken by the cancer cell compared to the non-targeted NPs. This was due to the receptor-mediated endocytosis of the targeted NPs. Targeted NPs functionalized with CTX effectively bind with EGFR receptors overexpressed to the lung cancer cells, are transported inside the cells, and release their loaded content for anticancer activity. Whereas, nontargeted NPs were uptaken by the cells via passive diffusion (186).

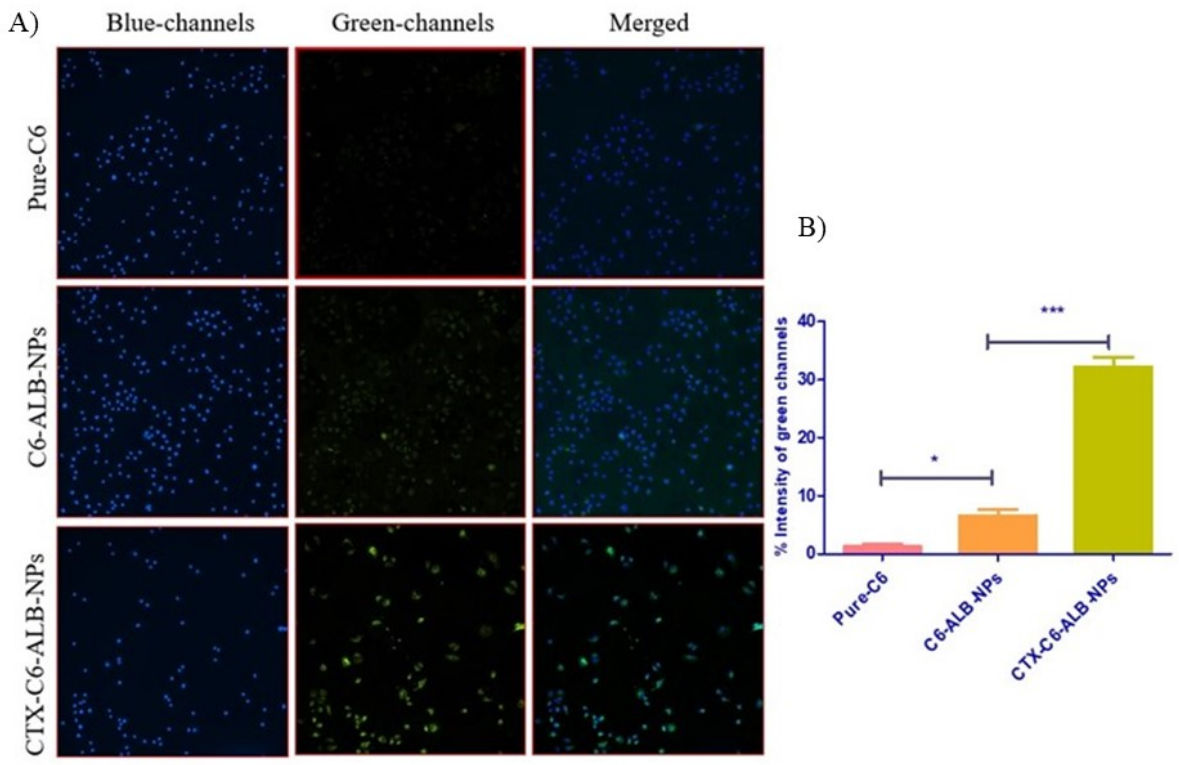

Figure 36 A) Cellular-uptake images of pure C6 and C6 loaded non-targeted and CTX conjugated ALB-NPs, and B) Percent intensity of green channels in cellular-uptake images

4.10.4 Acridine orange/ethidium bromide staining for detection of apoptosis in A549 cells

This research work utilized the AO/EtBr staining assay with the MTT assay to determine whether ALB-NPs-mediated cell death occurs through apoptosis or necrosis The presence of apoptosis can be quantified using a nuclear staining assay, which involves observing specific morphological features such as nucleus breakdown, fragmented chromatin, nuclear envelope destruction, and cell blebbing. In our study, we stained the nuclei with AO and EtBr to observe the apoptotic cell population after treatment with ALB-NPs. Our results confirmed that the synthesized NPs (ALB-NPs) induced maximum chromatin condensation and cell shrinkage in A549 cells. In the case of the A549 cell line, ALB-NPs treated cells induced more nuclear fragmentation and cytoplasmic shrinkage. Our study reveals that viable cells exhibit green fluorescence and display uniform chromatin with an intact cell membrane, while early

apoptosis is indicated by nuclear fragmentation (Fig. 37). Cells in late apoptosis were characterized by condensed or fragmented chromatin, with nuclei exhibiting orangish or pale-yellow fluorescence. The research findings demonstrated that the synthesized NPs primarily triggered cell death via apoptosis, which highlights the strong potential of ALB-NPs as an effective anticancer agent. The study results also established that A549 cells exhibited varying sensitivity to CTX-ASA-ALB-NPs compared to ASA-ALB-NPs and ASA alone. Consequently, based on the AO/EtBr double staining analysis findings, it can be inferred that CTX-ASA-ALB-NPs triggered apoptosis more effectively than ASA, potentially due to their targeted action on lung cancer cells. CTX-ASA-ALB-NPs resulted in greater apoptosis in A549 cells compared to free ASA and ASA-ALB-NPs due to the targeted delivery of the loaded ASA to the cancer cells via receptor-mediated transcytosis.

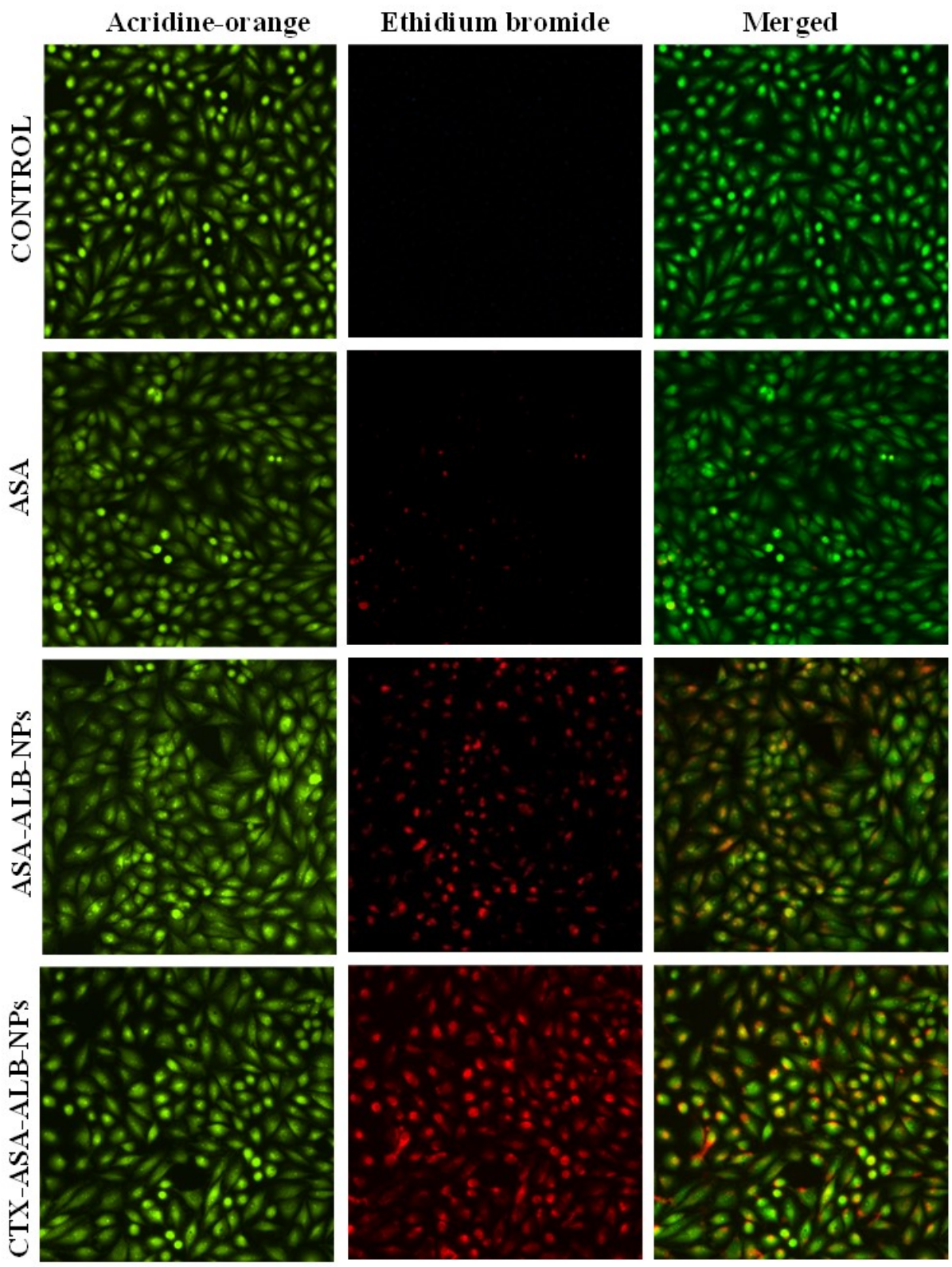

Figure 37 Cells morphological changes after treatment of free ASA, ASA-ALB-NPs and CTX-ASA-ALB-NPs in A549 cells

4.10.5 AnnexinV-Alexa fluor/Propidium iodide staining assay

In this research study, A549 cells were treated with ASA, ASA-ALB-NPs, and CTX-ASA-ALB-NPs at a consistent concentration of 11.61 µg/ml for 24 h to determine their quantitative effect on inducing apoptosis. The results of the flow cytometric analysis are presented in Fig. 38, which depicts the impact of treating A549 cells with ASA, ASA-ALB-NPs, and CTX-ASA-ALB-NPs for 24 h at equivalent drug concentrations, followed by dual staining with annexin V- Alexa fluor and propidium iodide. Analysis of Fig. 38 revealed that the percentage of total apoptotic cells was 17.6 ± 1.4%, 34.29 ± 1.7%, and 66.7 ± 2.1% in cells treated with ASA, ASA-ALB-NPs, and CTX-ASA-ALB-NPs, respectively (n = 3). After treatment with ASA, ASA-ALB-NPs, and CTX-ASA-ALB-NPs, the necrotic populations within the cell population were determined to be 1.5 ± 1.2%, 3.1 ± 1.7%, and 2.8 ± 1.4%, respectively (n = 3). These findings suggest that CTX-ASA-ALB-NPs have a greater potential to induce apoptosis and exert cytotoxic effects on human lung cancer cells (A549) than ASA and ASA-ALB-NPs.

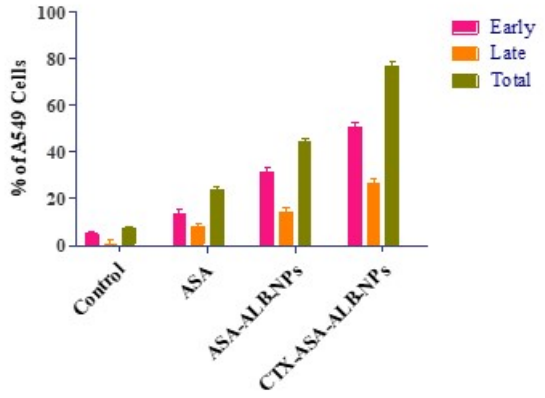

Figure 38 A) Flow cytometric analysis of control and treated A549 cells with same concentrations of ASA, ASA-ALB-NPs, and CTX-ASA-ALB-NPs. Dual staining with AnnexinV/PI distinguishes the percentage of cells at various phases. B) Statistical analysis has been performed using one-way ANOVA followed by Tukey test where a, b and c represents comparison between early, late and total population of control group to early, late and total apoptotic population of experimental groups respectively. Here *, ** and *** represents significant difference at $p < 0.05$, 0.01 and 0.001 respectively as compared to control

4.10.6 Cell cycle analysis

The cell cycle typically progresses through four distinct phases, namely G1, S, G2, and M. Targeting specific stages of the cell cycle is a promising approach in developing anti-cancer drugs to treat this debilitating disease.

The effect of ASA-ALB-NPs and CTX-ASA-ALB-NPs at a concentration of 11.61 µg/mL on cell cycle progression in A549 cells was assessed by flow cytometry after 24 h of exposure. Fig. 39 displays a representative cell cycle grid of stained DNA, demonstrating the distribution of cells across the sub-G1, S, G0-G1, and G2/M phases of the cycle. The findings from the study indicated that ASA-ALB-NPs, and CTX-ASA-ALB-NPs primarily caused blockage at the G1 phase of the cell cycle of A549 cells as the G0/G1 ratio increased to 71.5 ± 1.4%, and 80.1 ± 2.1% in ASA-ALB-NPs, and CTX-ASA-ALB-NPs treated cells respectively (n = 3), compared to the control cells (59.02 ± 1.8%). The outcomes of the study revealed the ability of CTX-ASA-ALB-NPs to arrest the cell cycle at the G0/ G1 phase.

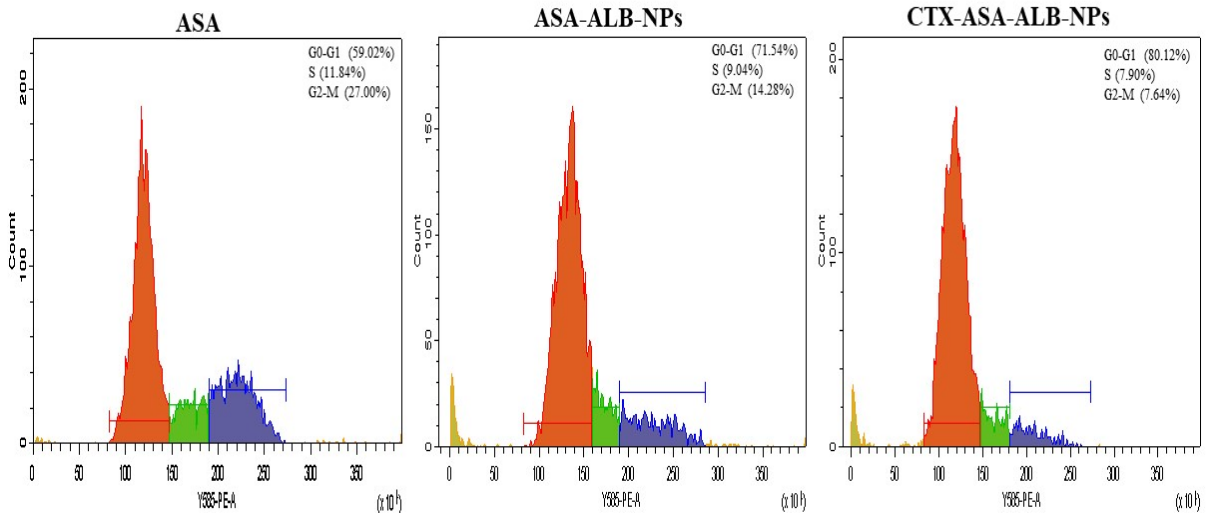

Figure 39 Distribution of cell cycle phases in A549 cells determined by flow cytometry using PI labeling (G0-G1, S and G2/M) after treatment with ASA-ALB-NPs, and CTX-ASA-ALB-NPs

4.11 *In vivo* studies

4.11.1 Pharmacokinetic Investigation

A pharmacokinetic study was conducted *in vivo* on wistar rats to investigate the efficacy of ASA control, ASA-ALB-NPs, and EGFR-targeted CTX-ASA-ALB-NPs. The concentration of ASA in plasma over time was plotted following intravenous administration of formulations containing equivalent concentrations of 10 mg/kg of ASA (Fig. 40).

The findings indicated a relative bioavailability of approximately 2 times higher for both ALB-NPs when compared to the ASA control. The pharmacokinetic profile analysis of CTX-ASA-ALB-NPs demonstrated a significant increase in both half-life and mean residence time when compared to the ASA control ($p < 0.05$).

The nanoparticle formulations displayed a substantially reduced rate of clearance in comparison to the ASA control (Table 13). A stealth effect imparted by TPGS present in the NPs may explain the improved residence time and half-life duration of ASA in the body. Hence, such modification in the formulation by TPGS prevents the opsonization of the NPs, improves the circulation time, and inhibits the Pgp efflux pump.

Table 13 Pharmacokinetic parameters of ASA and ASA-ALB-NPs, CTX-ASA-ALB-NPs

Parameters	Asiatic acid (Mean ± SD*)	ASA-ALB-NPs (Mean ± SD*)	CTX-ASA-ALB-NPs (Mean ± SD*)
AUC $_{total}$ (ng.h/ml)	36980.98± 1132.14	78681.29 ± 1463.45	83149.81 ± 1152.45
C_0 (ng/ml)	12419.78 ± 2122.35	10046.88 ± 1783.85	9251.99 ± 1853.62
$T_{1/2}$ (h)	8.95 ± 0.67	28.87 ± 3.46	31.63 ± 3.21
MRT (h)	6.22 ± 0.41	37.92 ± 4.61	42.56 ± 4.24
V_d (l/kg)	0.812 ± 0.03	0.647 ± 0.04	0.615 ± 0.03
Cl $_{total}$ (ml/kg.h)	62.90 ± 1.10	15.53 ± 0.87	13.50 ± 0.75
K_E (h^{-1})	0.077 ± 0.004	0.024 ± 0.002	0.022 ± 0.003
F_R	-	2.13	2.25

ASA: Asiatic acid, ASA-ALB-NPs: Asiatic acid-loaded ALB-NPs, CTX-ASA-ALB-NPs: CTX conjugated Asiatic acid loaded ALB-NPs, MRT: Mean residence time, V_d: Volume of distribution, Cl total: Total body clearance, C_{max}: maximum plasma concentration, Tmax: time to reach C_{max}; AUC total: area under plasma drug concentration-time curve; $T_{1/2}$: biological

half-life; K_E: Elimination rate constant (fraction of drug in an animal that is eliminated per unit of time), F_R: Relative bioavailability. *n = 3.

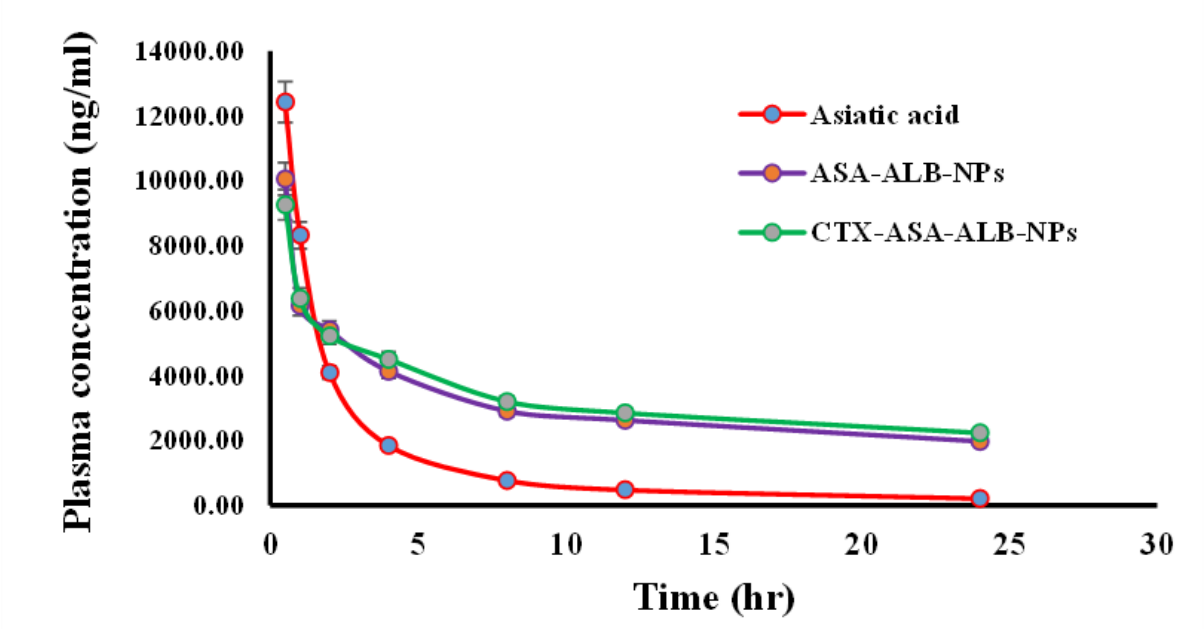

Figure 40 Pharmacokinetic analysis of ASA control, non-targeted, and EGFR targeted NPs after *i.v.* administration (10 mg/kg *i.v.*, n = 3) in Wistar rats

4.11.2 Histopathological evaluation

In our study, we did not observe any pathological abnormalities in the vital organs (heart, lungs, liver, and kidneys) of Wistar rats that were treated with the normal saline solution (control group). Physical observation of the rats suggested that there was no considerable toxicity within 14 days following the *i.v.* injection of ALB-NPs (Fig 41). Moreover, the histopathological evaluation suggested that the ASA group showed few lesions in cardiac tissue and liver tissue, whereas none were detected in the CTX-ASA-ALB-NPs group. The outcome indicates that TPGS has enhanced the compatibility of CTX-ASA-ALB-NPs with lung tissue.

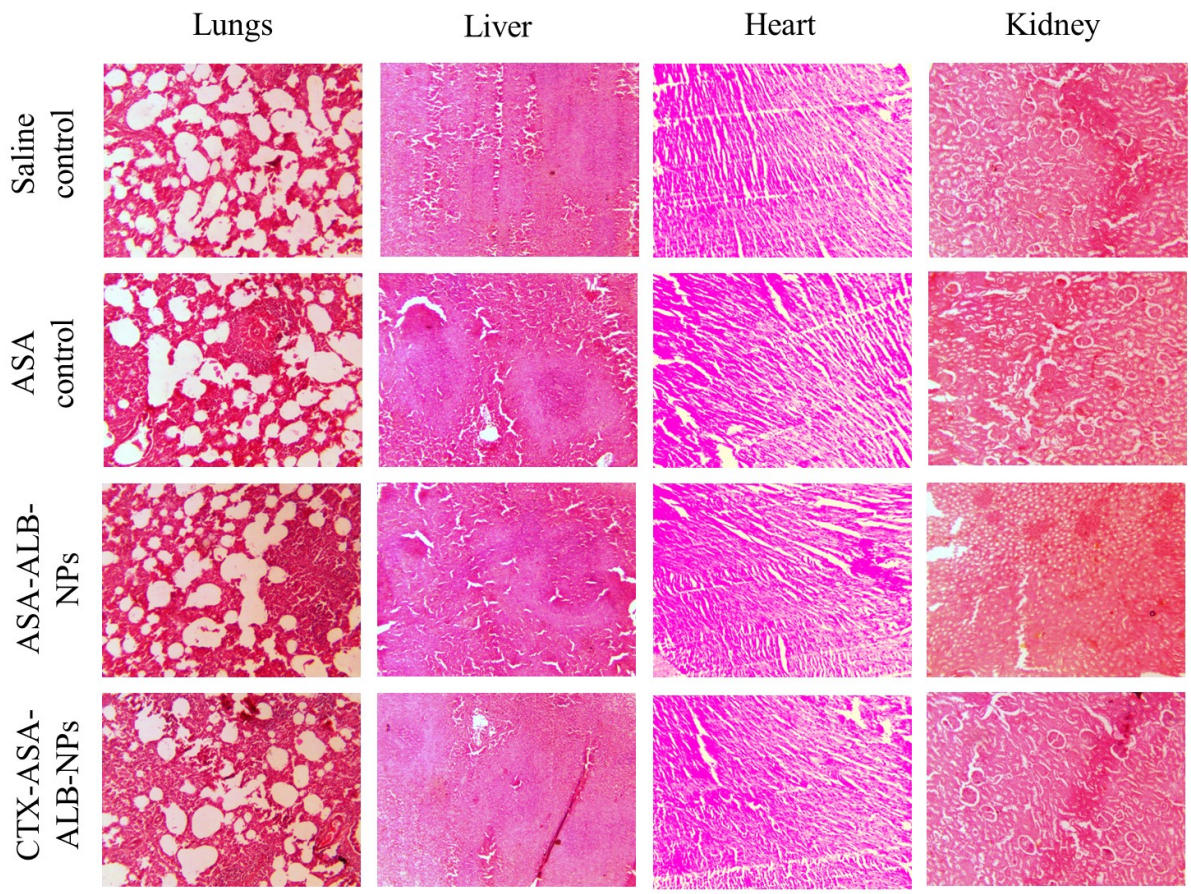

Figure 41 H&E-stained microscopic images of vital organs of animals treated with Saline control, ASA control, non-targeted ASA-ALB-NPs, and targeted CTX- ASA-ALB-NPs

5. Conclusion

In the current research work, we have formulated ALB nanoparticles containing asiatic acid and conjugated them with CTX, with the goal of improving the efficacy of lung cancer treatment. The EGFR-targeted NPs were prepared to get an improved and selective therapeutic efficacy against lung cancer.

The physicochemical properties of the optimized batch of ALB-NPs were assessed. In this research study, the particle size, PDI, and surface charge values of the ALB-NPs were evaluated, and they were found to fall within acceptable ranges. Furthermore, CTX-conjugated NPs exhibited marginally lower entrapment efficiency than non-targeted formulations. Targeted NPs were found to contain CTX on their surface based on the results of the XPS

survey. Moreover, *in vitro* studies revealed controlled and sustained release profiles for the prepared NPs and their pH-dependent drug release characteristics. The findings of *in vitro* investigations utilizing the MTT assay, apoptosis assay, and cell cycle analysis have demonstrated that ASA-ALB-NPs and CTX-ASA-ALB-NPs exhibit considerable cytotoxicity against lung cancer cells, surpassing the efficacy of free ASA. The apoptotic studies and cell cycle analysis collectively confirmed that CTX-ASA-ALB-NPs show higher anticancer activity than ASA. The improved delivery of entrapped ASA by the nanoparticles may be responsible for the increased cytotoxicity and more excellent induction of apoptosis.

Pharmacokinetic and histopathological investigations on Wistar rats demonstrated extended efficacy, improved absorption, and enhanced safety. Our hypothesis proposes that the augmented accumulation of CTX-ASA-ALB-NPs within lung cancer cells induces cytotoxicity, thereby contributing to its efficacious therapeutic efficiency. In summary, the findings indicate that ALB-NPs have the potential to serve as an outstanding nanocarrier for transporting hydrophobic drugs, such as Asiatic acid, and enhancing their anticancer efficacy against lung cancer cells.